Synthesis and Crystal and Electronic Structures of the Dinuclear Platinum Compounds $[PEtPh_3]_2[Pt_2(\mu\text{-}PPh_2)_2(C_6F_5)_4]$ and $[Pt_2(\mu\text{-}PPh_2)_2(C_6F_5)_4]$: A Computational Study by Density Functional Theory†

Ester Alonso,‡ José M. Casas,‡ F. Albert Cotton,*,§ Xuejung Feng,§ Juan Forniés,*,‡ Consuelo Fortuño,‡ and Milagros Tomas‡

Departamento de Química Inorgánica and Instituto de Ciencia de Materiales de Aragón, Universidad de Zaragoza−CSIC, 50009 Zaragoza, Spain, and Department of Chemistry and Laboratory for Molecular Structure and Bonding, Texas A&M University, College Station, Texas 77843

Received December 16, 1998

The electrolytic behavior of the dinuclear complexes $[NBu_4]_2[MM'(\mu\text{-}PPh_2)_2(C_6F_5)_4]$ (M = M′ = Pt (**1**), Pd (**1a**); M = Pt, M′ = Pd (**1b**)) has been studied, showing electrochemically irreversible oxidation and related reduction processes. The chemical oxidation of the binuclear compound for M = M′ = Pt, results in the formation of the binuclear Pt(III) compound $[Pt_2(\mu\text{-}PPh_2)_2(C_6F_5)_4]$. The crystal structure analysis of both complexes has been carried out, showing very similar structures with similar Pt−C and Pt−P distances and analogous skeletons. However the Pt−Pt distances are very different, 3.621(1) Å for the Pt(II) compound and 2.7245(7) Å for the Pt(III) derivative (as are the parameters geometrically related to this Pt−Pt distance), suggesting that, in the Pt(III) compound, there is a strong Pt−Pt bond. Results of DFT calculations on $[Pt_2(\mu\text{-}PH_2)_2(C_6F_5)_4]^{n-}$ (n = 2, 0) agree very well with the crystallographic data and indicate that, in the Pt(III) compound, there is approximately a single σ bond between the metal atoms.

Introduction

The well-known flexibility of the bridging phosphido μ-PR_2 groups has made these ligands very versatile in the synthesis of metal clusters with a wide range of bonding and nonbonding M−M distances supported by the μ-PR_2 ligands[1] and with unusual bonding situations.[2]

The flexibility of these phosphido ligands allows easy closing up of the metal centers, depending on the total valence electron count, in order to form metal−metal bonds. In a phosphido complex of this type, the total valence electron count can be modified either by adding or eliminating ligands from the framework[1b] or through oxidation−reduction processes of the metal centers, which often result in a large change in the metal−metal distances and consequently of the M−P−M bond angle.[3]

We have synthesized the dinuclear $[NBu_4]_2[MM'(\mu\text{-}PPh_2)_2(C_6F_5)_4]$ (M = M′ = Pt (**1**), Pd (**1a**); M = Pt, M′ = Pd (**1b**))[1a] complexes and studied their reactivity, which allows the synthesis of a great variety of polynuclear phosphido complexes with the metal centers in formal oxidation state II and with or without metal−metal bonds.

In this paper, we study the electrolytic behavior of these dinuclear complexes and report the chemical synthesis of the platinum(III) neutral dinuclear derivative $[Pt_2(\mu\text{-}PPh_2)_2(C_6F_5)_4]$ [bis(μ-diphenylphosphanido)bis[bis(pentafluorophenyl)platinum-(III)] (*Pt−Pt*)] (**2**) by oxidation of the Pt(II) compound **1** [tetra-*n*-butylammonium bis(μ-diphenylphosphanido)bis[bis(pentafluorophenyl)platinate(II)]. The crystal structures of complexes **1** and **2** established by X-ray diffraction methods as well as a study of the structural and electronic properties of these compounds carried out by means of density functional theory (DFT) are reported in this paper.

† Polynuclear Homo- or Heterometallic Palladium(II)−Platinum(II) Pentafluorophenyl Complexes Containing Bridging Diphenylphosphido Ligands. 7. For part 6, see ref 3a.

‡ Universidad de Zaragoza.

§ Texas A&M University.

(1) (a) Forniés, J.; Fortuño, C.; Navarro, R.; Martínez, F.; Welch, A. J. *J. Organomet. Chem.* **1990**, *394*, 643. (b) Falvello, L. R.; Forniés, J.; Fortuño, C.; Martínez, F. *Inorg. Chem.* **1994**, *33*, 6242. (c) Alonso, E.; Forniés, J.; Fortuño, C.; Martín, A.; Rosair, G. M.; Welch, A. J. *Inorg. Chem.* **1997**, *36*, 4426. (d) Alonso, E.; Forniés, J.; Fortuño, C.; Tomás, M. *J. Chem. Soc., Dalton Trans.* **1995**, 3777. (e) Baker, R. T.; Fultz, W. C.; Marder, T. B.; Williams, I. D. *Organometallics* **1990**, *9*, 2357. (f) Bender, R.; Braunstein, P.; Dedieu, A.; Ellis, P. D.; Huggins, B.; Harvey, P. D.; Sappa, E.; Tiripicchio, A. *Inorg. Chem.* **1996**, *35*, 1223. (g) Leoni, P.; Manetti, S.; Pasquali, M.; Albinati, A. *Inorg. Chem.* **1996**, *35*, 6045. (h) Leoni, P.; Manetti, S.; Pasquali, M. *Inorg. Chem.* **1995**, *34*, 749. (i) Powell, J.; Sawyer, J. F.; Stainer, M. V. R. *Inorg. Chem.* **1989**, *28*, 4461. (j) Powell, J.; Fuchs, E.; Gregg, M. R.; Phillips, J.; Stainer, M. V. R. *Organometallics* **1990**, *9*, 387. (k) Morrison, E. D.; Harley, A. D.; Marcelli, M. A.; Geoffroy, G. L.; Rheingold, A. L.; Fultz, W. C. *Organometallics* **1984**, *3*, 1407. (l) Deeming, A. J.; Doherty, S. *Polyhedron* **1996**, *15*, 1175.

(2) (a) Alonso, E.; Forniés, J.; Fortuño, C.; Martín, A.; Orpen, A. G. *J. Chem. Soc., Chem. Commun.* **1996**, 231. (b) Bender, R.; Braunstein, P.; Dedieu, A.; Dusausoy, Y. *Angew. Chem., Int. Ed. Engl.* **1989**, *28*, 923. (c) Gol, F.; Knuppel, P. C.; Stelzer, O.; Sheldrick, W. S. *Angew. Chem., Int. Ed. Engl.* **1988**, *27*, 956. (d) Brauer, D. J.; Knuppel, P. C.; Stelzer, O. *J. Chem. Soc., Chem. Commun.* **1988**, 551. (e) Jones, R. A.; Stuart, A. L.; Wright, T. C. *J. Am. Chem. Soc.* **1983**, *105*, 7459. (f) Leoni, P.; Pasquali, M.; Pieri, G.; Albinati, A.; Pregosin, P. S.; Ruegger, H. *Organometallics* **1995**, *14*, 3143. (g) Leoni, P.; Pieri, G.; Pasquali, M. *J. Chem. Soc., Dalton Trans.* **1998**, 657. (h) Leoni, P.; Pasquali, M.; Sommonigo, M.; Laschi, F.; Zanella, P.; Albinati, A.; Lianza, F.; Pregosin, P. S.; Ruegger, H. *Organometallics* **1993**, *12*, 1702. (i) Leoni, P.; Pasquali, M.; Sommonigo, M.; Albinati, A.; Pregosin, P. S.; Ruegger, H. *Organometallics* **1996**, *15*, 2047.

(3) (a) Falvello, L. R.; Forniés, J.; Fortuño, C.; Martín, A.; Martínez-Sariñena, A. P. *Organometallics* **1997**, *16*, 5849. (b) Shyn, S.-G.; Lin, P.-J.; Wen, Y.-S. *J. Organomet. Chem.* **1993**, *443*, 115. (c) Shyn, S.-G.; Hsu, J.-Y.; Wen, Y.-S. *J. Organomet. Chem.* **1993**, *453*, 97.

10.1021/ic981437z CCC: $18.00
Published on Web 10/08/1999

Experimental Section

C, H, and N analyses and IR, NMR, and mass spectroscopies were performed as described elsewhere.[1c] Literature methods were used to prepare the starting material $[NBu_4]_2[Pt_2(\mu\text{-}PPh_2)_2(C_6F_5)_4]$.[1a] $[PEtPh_3]_2[Pt_2(\mu\text{-}PPh_2)_2(C_6F_5)_4]$ (**1′**) (for X-ray purposes exclusively) was prepared similarly but using $[PEtPh_3][ClO_4]$ instead of $[NBu_4][ClO_4]$.

Cyclic voltammetric studies were performed using an EG&G model 273 potentiostat in conjunction with a three-electrode cell. The three-electrode system consists of a platinum disk working electrode, a platinum wire auxiliary electrode, and a saturated calomel reference electrode (SCE) separated from the test compartment by a fine-porosity frit. The measurements were carried out in CH_2Cl_2 solutions 5×10^{-4} M in the test compounds and 0.1 M in $[NBu_4][PF_6]$ as supporting electrolyte. Under the conditions used, the $E°$ value for the couple $[Fe(\eta^5\text{-}C_5H_5)_2]^+/[Fe(\eta^5\text{-}C_5H_5)_2]$ was 0.47 V.

Safety note: Perchlorate salts of metal complexes with organic ligands are potentially explosive. Only small amounts of material should be prepared, and these should be handled with great caution.

Preparation of $[Pt_2(\mu\text{-}PPh_2)_2(C_6F_5)_4]$ (2). To a solution of $[NBu_4]_2[Pt_2(\mu\text{-}PPh_2)_2(C_6F_5)_4]$ (0.500 g, 0.261 mmol) in CH_2Cl_2 (30 mL) was added $AgClO_4$ (0.109 g, 0.525 mmol), and the mixture was stirred, at room temperature and in the dark, for 3 h. The resulting yellow solution was filtered through Celite, and the filtrate was evaporated to dryness. The oily yellow residue was treated with Et_2O (15 mL) to precipitate the insoluble NBu_4ClO_4, and the solution was evaporated to dryness. The residue was treated with 5 mL of CH_2Cl_2, and the mixture was kept in a freezer (−20 °C) for 5 h. The resulting yellow crystals (**2**) were filtered off and washed with 2 × 0.5 mL of cold CH_2Cl_2 (0.280 g, 75% yield). Anal. Found (calcd for $C_{48}F_{20}H_{20}P_2Pt_2$): C, 40.01 (40.35); H, 1.40 (1.41). IR (C_6F_5, cm^{-1}): ν(C−F) 964; X-sensitive 790, 781. FAB^+ MS: *m*/*z* 1428 ($C_{48}F_{20}H_{20}P_2Pt_2$). ^{19}F NMR ($CDCl_3$), δ: −119.4 (8 *o*-F, $^3J_{Pt,F} = 394.6$ Hz), −157.3 (8 *m*-F), −161.8 (4 *p*-F) ppm. $^{31}P\{^1H\}$ NMR ($CDCl_3$), δ: 281.7 (s, $^1J_{Pt,P} = 1224.3$ Hz) ppm.

Reaction of 2 with NBu_4BH_4. To a yellow solution of **2** (0.100 g, 0.070 mmol) in CH_2Cl_2 (5 mL) was added NBu_4BH_4 (0.036 g, 0.140 mmol), and the mixture was stirred for 1 h. The solution was evaporated to dryness, and *i*-PrOH (10 mL) was added. After 2 h of stirring, complex **1** was filtered off and washed with 2 × 0.5 mL of *i*-PrOH (0.054 g, 40% yield).

Crystal Structure Determinations of $[PEtPh_3]_2[Pt_2(\mu\text{-}PPh_2)_2(C_6F_5)_4]$ (1′) and $[Pt_2(\mu\text{-}PPh_2)_2(C_6F_5)_4]$ (2). Suitable crystals of **1′** and **2** for X-ray purposes were obtained by slow diffusion of *n*-hexane into solutions of 0.015 g of $[PEtPh_3]_2[Pt_2(\mu\text{-}PPh_2)_2(C_6F_5)_4]$ in acetone (3 mL) and 0.025 g of $[Pt_2(\mu\text{-}PPh_2)_2(C_6F_5)_4]$ in CH_2Cl_2 (3 mL), respectively, at 4 °C.

Data for both compounds were acquired on a Siemens/Stoe AED2 diffractometer. Some important crystal data are summarized in Table 1. The intensity data were collected by the $\omega-\theta$ scan technique. Three check reflections were measured every 180 (**1′**) or 90 (**2**) min, and they showed no decay. The intensity data were corrected for Lorentz and polarization effects and for absorption (ψ scan methods). No extinction correction was applied. The positions of the heavy atoms were determined from a Patterson map.[4] The structures were developed using full-matrix least-squares refinements and difference Fourier syntheses.[5] The H atoms of the phenyl groups were incorporated at calculated positions and refined with a riding model in which the C−H distances were fixed at 0.96 Å and with isotropic displacement parameters of 1.2 times the equivalent isotropic displacement parameters of the respective bonded C atoms.

Compound **1′** crystallizes in space group $P2_1/n$, with $Z = 2$. There is only one-half anion and one $[PEtPh_3]^+$ cation in the asymmetric unit. The CH_3 group of the ethyl moiety is disordered over two positions (C(71A) and C(71B)) with an occupancy factor of 0.5 for each one. No H atoms of the ethyl group were included. All non-hydrogen atoms, including those of the disordered methyl group, were refined with anisotropic displacement parameters. Convergence of the least-squares refinement based on F^2 was indicated by a maximum shift/error for the last cycle: 0.009 for U_{22} of C_{70}. Largest difference peak and hole: 0.47 and −0.33 e/Å^3.

Table 1. Crystallographic Data for $[PEtPh_3]_2[Pt_2(\mu\text{-}PPh_2)_2(C_6F_5)_4]$ (**1′**) and $[Pt_2(\mu\text{-}PPh_2)_2(C_6F_5)_4]\cdot 2CH_2Cl_2$ (**2**·$2CH_2Cl_2$)

	1′	**2**·$2CH_2Cl_2$
empirical formula	$C_{88}H_{60}F_{20}P_4Pt_2$	$C_{50}H_{24}Cl_4F_{20}P_2Pt_2$
fw	2011.42	1598.62
a , Å	14.508(3)	21.780(7)
b, Å	13.904(4)	10.468(3)
c , Å	19.799(5)	24.234(6)
α, deg	90	90
β, deg	93.60(2)	114.08(2)
γ, deg	90	90
V, Å^3	3962(2)	5044(3)
space group	$P2_1/n$	$I2/a$
Z	2	4
D_{calc}, Mg/m^3	1.676	2.105
crystal size, mm	0.40 × 0.25 × 0.25	0.25 × 0.25 × 0.20
abs coeff, mm^{-1}	3.679	5.928
λ, Å	0.710 73	0.710 73
temp, K	293(2)	210(2)
transm factors	0.284−0.231	0.985−0.619
final *R* indices [$I > 2\sigma(I)$]: R1,[a] wR2[b]	0.0313, 0.0615	0.0310, 0.0691
R indices (all data): R1,[a] wR2[b]	0.0520, 0.0678	0.0481, 0.0784

[a] $R1 = \sum||F_o| - |F_c||/\sum|F_o|$. [b] $wR2 = [\sum w(F_o^2 - F_c^2)^2/\sum w(F_o^2)^2]^{1/2}$.

Compound **2** crystallizes in space group $I2/a$ (No. 15), with $Z = 4$, and there is one-half molecule in the asymmetric unit. The asymmetric unit also contains a CH_2Cl_2 solvent molecule. All non-hydrogen atoms, including those of the solvent molecule, were refined with anisotropic displacement parameters. The maximum shift/error for the last cycle was 0.116 for U_{22} of Cl_2. Largest difference peak and hole: 0.69 and −0.82 e/Å^3.

Computational Procedures. DFT calculations were carried out for $[Pt_2(\mu\text{-}PH_2)_2(C_6F_5)_4]^{n-}$ ($n = 2, 0$) in which the bridging ligand, PPh_2, of the title compounds was replaced by PH_2. The calculations utilized Becke's hybrid methods,[6a] B3PW91 and B3LYP, which include the Perdew−Wang 1991[6b] and the Lee−Yang−Parr[6c] gradient-corrected correlation functionals, respectively, for nonlocal correlation. DFT calculations with the local spin density approximation, SVWN, were also performed by using the Slater exchange and the Vosko−Wilk−Nusair correlation functional.[6d]

The calculations employed relativistic core potentials and the associated LANL2DZ basis set[7] for the platinum atoms. All-electron basis sets residing in the Gaussian 94 program[8] were used for all other atoms, namely, 6-31G(d) for phosphorus (6D keyword, 490 basis functions) and 6-31G for C, F, and H. Molecular structures of the model compounds were obtained by complete geometry optimization in D_{2h} symmetry. The optimized structures are shown by drawings generated with the SHELXL-93 program.[9] All computations were carried on SGI Power Challenge computers.

(4) Calculations were carried out on a Local Area VAXcluster (VAX/VMS V5.5) with the program REDU4, Revision 7.03 (Stoe), for data reduction and with the commercial package SHELXTL-PLUS, Release 4.21/V (Siemens), for structure solution.

(5) Structure refinement: Sheldrick, G. M. SHELXL-93: FORTRAN program for crystal structure refinement. University of Gottingen, 1993.

(6) (a) Becke, A. D. *J. Chem. Phys.* **1993**, *98*, 5648. (b) Perdew, J. P.; Wang, Y. *Phys. Rev.* **1992**, *B45*, 13244. (c) Lee, C.; Yang, W.; Parr, R. G. *Phys. Rev.* **1988**, *B37*, 785. (d) Vosko, S. H.; Wilk, L.; Nusair, M. *Can. J. Phys.* **1980**, *58*, 1200.

(7) Wadt, W. R.; Hay, P. J. *J. Chem. Phys.* **1985**, *82*, 284.

(8) Frisch, M. J.; Trucks, G. W.; Schegel, H. B.; Gill, P. M. W.; Johnson, G.; Robb, M. A.; Cheeseman, J. R.; Keith, T. A.; Petersson, G. A.; Montgomery, J. A.; Raghavachari, K.; Al-Laham, M. A.; Zakrzewski, V. G.; Ortiz, J. V.; Foresman, J. B.; Peng, C. Y.; Ayala, P. Y.; Wong, M. W.; Andres, J. L.; Replogle, E. S.; Gomperts, R.; Martin, R. L.; Fox, D. J.; Binkley, J. S.; Defrees, D. J.; Baker, J.; Stewart, J. P.; Head-Gordon, M.; Gonzalez, C.; Pople, J. A. *Gaussian 94*, Revision D3; Gaussian Inc.: Pittsburgh, PA. 1995.

(9) Sheldrick, G. M. In *Crystallographic Computing 6*; Falck, H. D., Parkanyi, L., Simon, K., Eds.; Oxford University Press: Oxford, U.K., 1993.

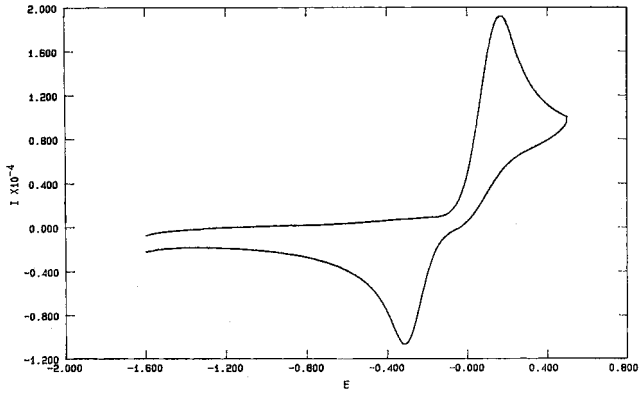

Figure 1. Voltammogram for the complex $[NBu_4]_2[Pt_2(\mu\text{-}PPh_2)_2(C_6F_5)_4]$.

Results and Discussion

Electrochemical Studies. The complexes $[NBu_4]_2[Pt_2(\mu\text{-}PPh_2)_2(C_6F_5)_4]$ (**1**), $[NBu_4]_2[Pd_2(\mu\text{-}PPh_2)_2(C_6F_5)_4]$ (**1a**), and $[NBu_4]_2[PtPd(\mu\text{-}PPh_2)_2(C_6F_5)_4]$ (**1b**) were studied by cyclic voltammetry. In all cases, the experiments were carried out in CH_2Cl_2 using $[NBu_4][PF_6]$ as the supporting electrolyte, a Pt disk electrode, and a calomel reference electrode (SCE). The complexes exhibit quite similar cyclic voltammograms, showing an electrochemically irreversible oxidation and a related reduction process in the range between −1.6 and 0.8 V. The oxidation waves appear at 0.37, 0.01, and 0.19 V, while the reduction waves are at −0.51, −0.62, and −1.07 V for complexes **1**, **1a**, and **1b**, respectively, and no further waves were observed in the range between −1.6 and +1.6 V. Figure 1 shows the voltammogram for $[NBu_4]_2[Pt_2(\mu\text{-}PPh_2)_2(C_6F_5)_4]$ in the range −0.16 to +0.5 V at a scan rate of 0.1 V s^{-1}.

Synthesis of $[Pt_2(\mu\text{-}PPh_2)_2(C_6F_5)_4]$ (2). According to the electrochemical studies, a colorless CH_2Cl_2 solution of $[NBu_4]_2[Pt_2(\mu\text{-}PPh_2)_2(C_6F_5)_4]$ was treated with $AgClO_4$ (1:2 molar ratio ($E^\circ_{Ag^+/Ag} = 0.799$ V) for 3 h, and the solution became intensely yellow, precipitating metallic silver. After filtration to eliminate the formed Ag^0, the dark yellow solution was evaporated to dryness, and the residue was treated with Et_2O to precipitate NBu_4ClO_4. From the mother liquor $[Pt_2(\mu\text{-}PPh_2)_2(C_6F_5)_4]$, **2** (75% yield), was obtained. The IR spectrum of **2** shows two bands assignable to the X-sensitive mode of the C_6F_5 groups, in accord with the presence of two C_6F_5 groups mutually cis per metal center. Moreover, the band of the C_6F_5 group which appears at 950 cm^{-1} for the platinum(II) precursor, is shifted toward higher wavelength in the spectrum of **2**, 964 cm^{-1}, as expected due to the increase of the formal oxidation state of the platinum centers.[10] The ^{19}F NMR spectrum shows three signals in a 2:1:2 intensity ratio, indicating that the four C_6F_5 groups are equivalent as are the two halves of each pentafluorophenyl group. In the $^{31}P\{^1H\}$ NMR spectrum of **2**, a singlet signal, with platinum satellites, is observed at higher chemical shift, 281.7 ppm, than the signal due to the starting material, −146.9 ppm. This low-field chemical shift is in accord with the presence of two PPh_2 ligands bridging two metal centers which are joined by a metal−metal bond, as we will see later.

Reactions of the analogous complexes $[NBu_4]_2[MM'(\mu\text{-}PPh_2)_2(C_6F_5)_4]$ (M = M′ = Pd (**1a**); M = Pt, M′ = Pd (**1b**)) with $AgClO_4$ under similar conditions result in the decomposition of the resulting solutions and formation of dark mixtures which we have not been able to separate or identify.

(10) Usón, R.; Forniés, J. *Adv. Organomet. Chem.* **1988**, *288*, 219.

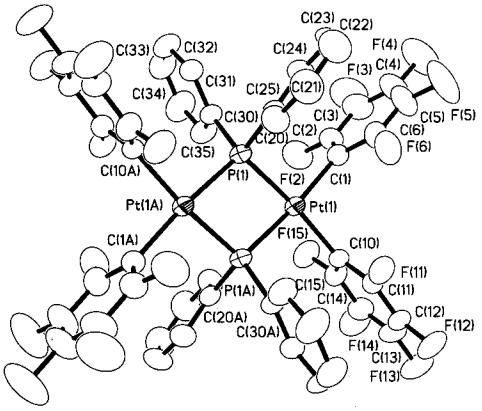

Figure 2. Crystal structure of the anion of complex **1′** showing the atom-labeling scheme.

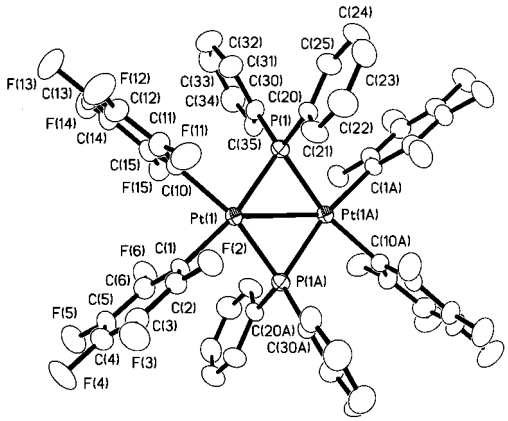

Figure 3. Crystal structure of **2** showing the atom-labeling scheme.

On the other hand, the dinuclear Pt(III) compound (**2**) can be chemically reduced to the Pt(II) compound by reaction with NBu_4BH_4 in CH_2Cl_2 in a 1:2 molar ratio.

Finally, compound **2** does not react with aqueous HCl in methanol or acetone, as does the analogous Pt(II) compound, which gives in this way the tetranuclear $[NBu_4]_2[(C_6F_5)_2Pt(\mu\text{-}PPh_2)_2Pt(\mu\text{-}Cl)_2Pt(\mu\text{-}PPh_2)_2Pt(C_6F_5)_2]$ compound. This lack of reactivity of **2** toward HCl can be understood by considering that these types of processes seem to take place through an oxidative addition reaction followed by a reductive elimination and that this Pt(III) compound cannot be further oxidized.

Crystal Structures of $[PEtPh_3]_2[(C_6F_5)_2Pt(\mu\text{-}PPh_2)_2Pt(C_6F_5)_2]$ (1′) and $[(C_6F_5)_2Pt(\mu\text{-}PPh_2)_2Pt(C_6F_5)_2]$ (2). The structures of the anion $[(C_6F_5)_2Pt(\mu\text{-}PPh_2)_2Pt(C_6F_5)_2]^{2-}$ and of $[(C_6F_5)_2Pt(\mu\text{-}PPh_2)_2Pt(C_6F_5)_2]$ obtained by X-ray diffraction studies are shown in Figures 2 and 3. Selected bond distances and angles are collected in Table 2. As can be seen, they display very similar dinuclear structures which are the result of the interaction of two identical *cis*-$(C_6F_5)_2Pt(\mu\text{-}PPh_2)$ fragments which form the planar dinuclear species with the platinum(II) or platinum(III) centers located in distorted square planar environments and the PPh_2 groups acting as typical bridging ligands. In both cases, the molecules sit on crystallographic inversion centers, and therefore the $Pt_2(\mu\text{-}PPh_2)_2$ cores are planar. Within each complex (**1′** and **2**), the two Pt−C distances are identical within experimental error, as are the two Pt−P distances. In addition, the Pt−C distances are identical in **1′** and **2**. The pentafluorophenyl rings are nearly perpendicular to the Pt_2P_2 plane, the dihedral angles between both planes being 86.4(2) and 78.6(2)° for **1′** and 85.0(2) and 82.8(2)° for **2**. The main difference in the structures of both compounds arises from

Table 2. Selected Bond Lengths (Å) and Angles (deg) for $[PEtPh_3]_2[Pt_2(\mu\text{-}PPh_2)_2(C_6F_5)_4]$ (**1′**) and $[Pt_2(\mu\text{-}PPh_2)_2(C_6F_5)_4]$ (**2**)

	1′	**2**
Pt(1)−C(1)	2.083(6)	2.085(6)
Pt(1)−C(10)	2.088(5)	2.076(6)
Pt(1)−P(1)	2.313(2)	2.281(2)
Pt(1)−P(1A)	2.310(2)	2.274(7)
Pt(1)−Pt(1A)	3.621(1)	2.7245(7)
C(1)−Pt(1)−C(10)	91.4(2)	82.8(2)
C(1)−Pt(1)−P(1)	96.6(2)	166.0(2)
P(1)−Pt(1)−P(1A)	76.87(6)	106.53(5)
P(1A)−Pt(1)−C(10)	95.1(2)	165.9(2)
C(1)−Pt(1)−P(1A)	173.4(2)	86.8(2)
C(10)−Pt(1)-P(1)	171.1(2)	84.6(2)
Pt(1A)-P(1)−Pt(1)	103.13(6)	73.47(5)

Chart 1

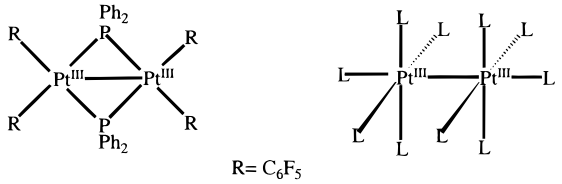

a **b**

the Pt−Pt distance, which is 2.7245(7) Å in **2** and 3.621(1) Å in **1′**. The formal oxidation states of the Pt centers in **2**, the diamagnetism of the compound, and the short Pt−Pt distance indicate the existence of a Pt−Pt bond. However, this distance is in the high end of the range of Pt(III)−Pt(III) distances found in other complexes with planar $Pt^{III}(\mu\text{-}X)_2Pt^{III}$ skeletons (2.570(1) Å in $[NBu_4]_2[Pt_2(\mu\text{-}C_6F_4O)_2(C_6F_5)_4]$; 2.584(1) Å in $[NBu_4]_2[Pt_2\{\mu\text{-}C_6F_4(OMe)_2\}_2(C_6F_5)_4]$; 2.611(2) Å in $[NBu_4]_2[Pt_2(\mu\text{-}C_6F_4Cl)(\mu\text{-}C_6F_5)(C_6F_5)_4]$.[11]

As expected, the Pt(II)−Pt(II) compound does not display a Pt−Pt bond and the Pt···Pt distance is much longer than that in complex **2**. As a consequence of the long Pt···Pt distance compared with the corresponding distance in the Pt(III)−Pt(III) compound, the Pt−P−Pt angles in **1′** are larger than the corresponding ones in complex **2**, showing the flexibility of the phosphido ligands. In addition and for geometrical reasons, larger Pt−P−Pt angles correspond to smaller values for P−Pt−P and vice versa, as can be seen from Table 2. This fact, which is obviously related to the Pt−Pt distance, influences the distortion of the square planar environment in both complexes.

Complex **2** is one of the very few existing Pt(III)−Pt(III) complexes which display coplanar platinum square planar coordination environments with the Pt−Pt bond and all the Pt−ligand bonds located in the same plane (see Chart 1a), since more frequently the Pt(III)−Pt(III) complexes display octahedral environments with the Pt−Pt bond perpendicular to the equatorial plane (see Chart 1b).[12]

The structural study of both complexes provides an excellent opportunity for comparing the effects of the two-electron oxidations on the metal−metal distances, since both systems display identical structures, with the only difference being in the metal to metal distances, which are dramatically different (as obviously are the parameters associated with them within the square $Pt_2(\mu\text{-}PPh_2)_2$). A similar behavior was observed for $[W_2(CO)_8(\mu\text{-}PPh_2)_2]$ and its two-electron-reduction compound

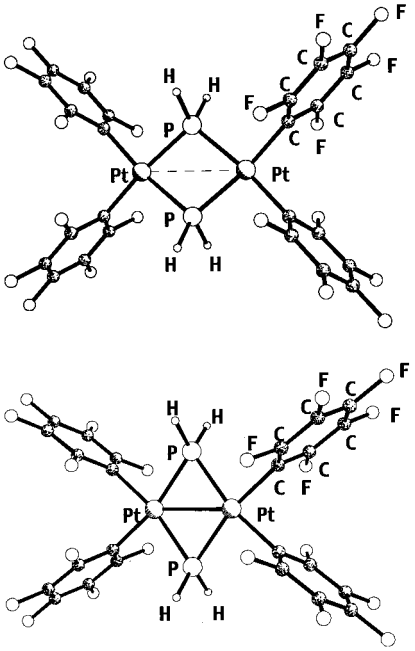

Figure 4. Optimized molecular structures of $[Pt_2(\mu\text{-}PH_2)_2(C_6F_5)_4]^{2-}$ (top) and $[Pt_2(\mu\text{-}PH_2)_2(C_6F_5)_4]$ (bottom).

$[Li(THF)_3]_2[W_2(CO)_8(\mu\text{-}PPh_2)_2]$,[13a] which present nearly identical structures, with important differences only in the W−W distances. In other cases, e.g. $[Fe_2(CO)_6(\mu\text{-}PPh_2)_2]$ and $[Na(2,2,2\text{-crypt})]_2[Fe_2(CO)_6(\mu\text{-}PPh_2)_2]$,[13b] which differ in two electrons as well, not only do the metal−metal distances change but also important differences in the geometry of the Fe_2P_2 core are observed.

Computational Study by Methods of Density Functional Theory. Molecular Structures. It has been shown that DFT methods are effective and very accurate for predicting molecular structures of dinuclear transition-metal complexes.[14] This is again evidenced by the optimized structures for both $[Pt_2(\mu\text{-}PH_2)_2(C_6F_5)_4]^{n-}$ ($n = 2, 0$) compounds (Figure 4), which compare well with the crystal structures for $[Pt_2(\mu\text{-}PPh_2)_2(C_6F_5)_4]^{n-}$ ($n = 2, 0$). Additional results from the DFT calculations of the molecular structures with the SVWN functional are shown in Table 3. It can be seen that both the very long and the short Pt-to-Pt distances are well reproduced. Other structural parameters, in particular, the bond angles, also compare satisfactorily with the experimental values.

Additional results of the structural calculations are given in Table 3, which contains also the optimized structural parameters from the B3LYP and B3PW91 calculations. We note that the hybrid methods with the nonlocal corrections correctly predict the two distinct Pt-to-Pt distances for the compounds, but the values of the distances are all significantly longer than those obtained from the SVWN calculations. In particular, the Pt-to-Pt separations optimized by the B3LYP method are about 0.1 Å too long in both calculated structures. The Pt−C distances calculated by the nonlocal methods, on the other hand, are considerably better than the SVWN results. DFT methods in the local density approximation, such as SVWN, are known to underestimate bond distances between transition-metal atoms and main-group atoms of the first row.[15]

(11) Usón, R.; Forniés, J.; Falvello, L. R.; Tomás, M.; Casas, J. M.; Martín, A.; Cotton, F. A. *J. Am. Chem. Soc.* **1994**, *116*, 7160.
(12) Cotton, F. A.; Walton, R. A. *Multiple Bonds between Metal Atoms*, 2nd ed.; Oxford University Press: Oxford, U.K., 1992.
(13) (a) Shyu, S.-G.; Calligaris, M.; Nardin, G.; Wojciki, A. *J. Am. Chem. Soc.* **1987**, *109*, 3617. (b) Ginsburg, R. E.; Rothrock, R. K.; Finke, R. G.; Collman, J. P.; Dahl, L. F. *J. Am. Chem. Soc.* **1979**, *101*, 6550.
(14) (a) Cotton, F. A.; Feng, X. *J. Am. Chem. Soc.* **1997**, *119*, 7514. (b) Cotton, F. A.; Feng, X. *J. Am. Chem. Soc*., submitted for publication.
(15) Ziegler, T. *Can. J. Chem*. **1995**, *73*, 743.

Table 3. Optimized Molecular Structures for $[Pt_2(\mu\text{-}PH_2)_2(C_6F_5)_4]^{n-}$ ($n = 2, 0$) with D_{2h} Averaged Experimental Data

	$[Pt_2(\mu\text{-}PH_2)_2(C_6F_5)_4]^{2-}$				$[Pt_2(\mu\text{-}PH_2)_2(C_6F_5)_4]$			
	B3LYP	B3PW91	SVWN	expt	B3LYP	B3PW91	SVWN	expt
				distances (Å)				
Pt−Pt	3.748	3.715	3.662	3.621(1)	2.811	2.771	2.718	2.724(1)
Pt−P	2.387	2.362	2.330	2.312(2)	2.317	2.297	2.275	2.278(2)
Pt−C	2.071	2.056	2.016	2.086(6)	2.087	2.073	2.036	2.081(6)
				Angles (deg)				
P−Pt−P	76.51	76.33	76.39	76.87(6)	105.27	105.80	106.65	106.53(5)
C−Pt−C	91.69	92.56	91.22	91.4(2)	83.42	83.73	81.12	82.8(2)
Pt−P−Pt	103.49	103.67	103.61	103.13(6)	74.73	74.20	73.35	73.47(5)
P−Pt−C	95.90	95.56	96.17	95.82(2)	85.66	85.23	86.12	85.7(2)

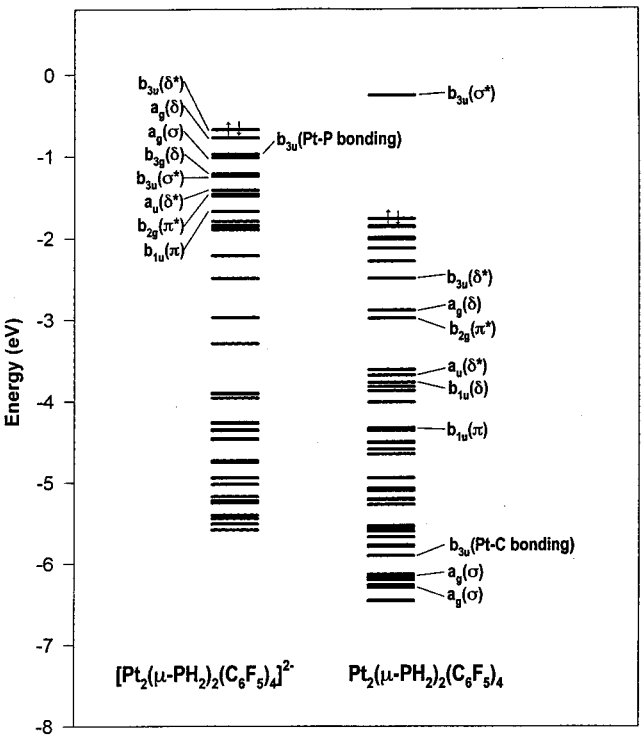

Figure 5. DFT orbital diagrams from calculations that afforded the results shown in Figure 4.

Electronic Structures and Metal−Metal Interactions. The large difference in the Pt-to-Pt distances in the two compounds naturally leads to interest in their electronic structures and the possibility of a direct metal−metal bonding interaction in the oxidized species. In the following, we will look at the calculated electronic structures of the compounds by analyzing the DFT orbitals. Before we start, it will be convenient to classify the metal orbitals according to the D_{2h} molecular symmetry and the coordinate system chosen for the calculations. In the coordinate system used for all DFT calculations, the metal atoms are located on the *X* axis, the phosphorus atoms on the *Y* axis, and the carbon atoms that are bonded to Pt on the *XY* plane. In other words, the $C_2Pt(\mu\text{-}P)_2PtC_2$ framework is in the *XY* plane. In such a coordinate system, the combinations of two $d_{x^2-y^2}$ orbitals of the metal atoms give rise to an a_g and a b_{3u} orbital (σ and σ^* type), the two d_{xz} orbitals give a b_{1u} and a b_{2g} orbital (π and π^* type), the two d_{yz} orbitals give a b_{3g} and an a_u orbital (δ and δ^* type), and the two d_{z^2} orbitals give rise to another pair of b_{3g} orbitals and an a_u orbital (δ and δ^* type). The combinations of d_{xy} orbitals, pointing directly to the ligands, on the other hand, have b_{2u} and b_{1g} symmetries and are totally involved in metal−ligand bonding.

Shown in Figure 5 are the diagrams of upper valence orbitals for $[Pt_2(\mu\text{-}PH_2)_2(C_6F_5)_4]^{2-}$ and $[Pt_2(\mu\text{-}PH_2)_2(C_6F_5)_4]$ in the optimized structures from the DFT calculations using the SVWN functional. The electronic structure for $[Pt_2(\mu\text{-}PH_2)_2(C_6F_5)_4]^{2-}$, which has a $Pt^{II}Pt^{II}$ core, is very much as expected. Among the highest occupied orbitals of this compound (see left column of Figure 5), eight have predominant contributions from the metal d orbitals and are labeled according to their symmetries and the types of combinations of the metal orbitals. Clearly, these orbitals are all within a small energy range, and their energies are not in the order that we frequently see in multiply bonded dinuclear compounds,[12] namely, $\sigma < \pi < \delta < \delta^* < \pi^* < \sigma^*$. Such a group of orbitals, therefore, may be best described as a block of d orbitals that accommodate 16 electrons from two well-separated, noninteracting metal centers. As an example, Figure 6a shows the $a_g(\sigma)$ Pt−Pt nonbonding orbital. The relative energies of the orbitals within the block are strongly affected

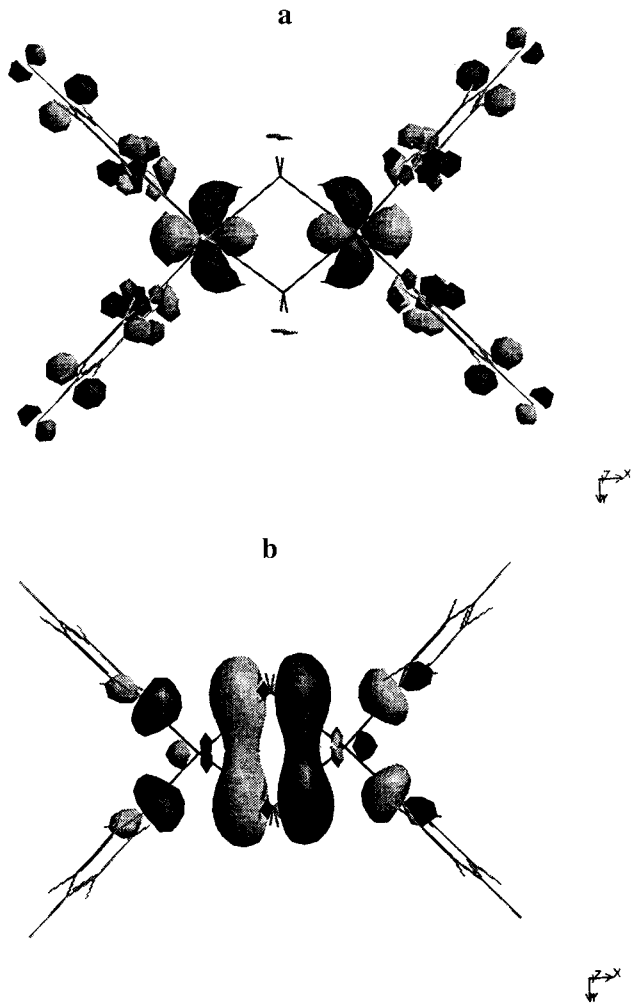

Figure 6. DFT orbital drawings for (a) the $a_g(\sigma)$ orbital and (b) the b_{3u} (Pt−P bonding) orbital in $[Pt_2(\mu\text{-}PH_2)_2(C_6F_5)_4]^{2-}$.

by secondary interactions between a metal atom and the ligands around it. Therefore, the orbital notations (σ, π, δ, etc.) are based on the types of d orbital combinations but do not indicate any significant metal−metal interactions.

For metal−ligand bonding, eight orbitals are required. In the coordinate system we described earlier, these comprise two orbitals from each of the a_g, b_{1g}, b_{2u}, and b_{3u} symmetry species. The actual situation, however, is much more complicated because of mixed characters of the orbitals of the same symmetry, which is very common in the calculations of such complicated molecular systems as we are dealing with here. We find that the contribution of the metal d orbitals (d_{xy}) to the Pt−P and Pt−C bonding is significant only for the bonding orbitals of b_{1g} and b_{2u} symmetries, as would be expected. For the metal−ligand bonding orbitals of a_g and b_{3u} symmetries, the calculations show extensive involvement of the 6s and 6p orbitals of the metal atoms. One example is the Pt−P bonding orbital of b_{3u} symmetry (see left column of Figure 5). The Pt−P bonding character of this orbital is shown in Figure 6b. This b_{3u} orbital is worthy of attention because of its correlation with the lowest unoccupied orbital in the oxidized compound, as we will see shortly.

The LUMO in $[Pt_2(\mu\text{-}PH_2)_2(C_6F_5)_4]^{2-}$ is a metal−ligand antibonding orbital and is not shown in Figure 5. The HOMO−LUMO gap is over 3 eV by this calculation. Therefore, the compound should have a well-defined closed-shell electronic configuration, which is consistent with the diamagnetism of the real compound. The calculation also supports the idea that oxidation of the Pt_2(II,II) compound should be expected to occur on the metal centers since the highest occupied orbitals are mainly metal-based orbitals that are close in energy. For the same reason, however, one may not be able to use the calculated results here to predict electronic structure and metal−metal interactions in the oxidation product which, as we already know, has gone through dramatic structural changes. As a matter of fact, as we will see below, along with the structural changes, the electron distribution in the oxidized species also undergoes rearrangement, and its electronic structure is indeed significantly different from that before oxidation.

Similar DFT orbitals for $[Pt_2(\mu\text{-}PH_2)_2(C_6F_5)_4]$ are shown by the right column in Figure 5. Notably, the highest occupied orbitals in this formal $Pt^{III}Pt^{III}$ compound are not metal based but are those of π orbitals on the C_6F_5 rings with the HOMO having b_{1g} symmetry. For the purpose of presentation, all orbitals in this column have been shifted upward by 5.4 eV so that the HOMO is aligned with the orbital of the same nature in the left column. At the Pt-to-Pt distance of 2.72 Å, one would expect significant interactions between the metal centers. This is indeed the case, as shown by the much increased energy separation between the orbital of Pt−Pt π bonding type, $b_{1u}(\pi)$, and its antibonding counterpart, namely, the $b_{2g}(\pi^*)$ orbital, though no net metal−metal bonding effects are expected. The four orbitals of δ and δ^* type are also totally metal-based orbitals. They, too, apparently do not contribute to metal−metal bonding.

The existence of metal−metal bonding in the oxidized compound is best shown by the facts that the energy of orbital of an $a_g(\sigma)$ type is much lower than those of all other metal-based orbitals and that this orbital has strong Pt−Pt σ-bonding character. As shown in the right column of Figure 5, the σ bonding splits into two $a_g(\sigma)$ orbitals because of nonbonding interactions of the metal orbital with ligand orbitals of the same symmetry. Both $a_g(\sigma)$ orbitals have substantial contributions from the metal atoms, and the one of mainly σ character and of higher energy is shown in Figure 7a. Such a Pt−Pt σ-bonding orbital may be compared with the Pt−Pt nonbonding $a_g(\sigma)$ orbital (Figure 6a) in the Pt_2(II,II) compound.

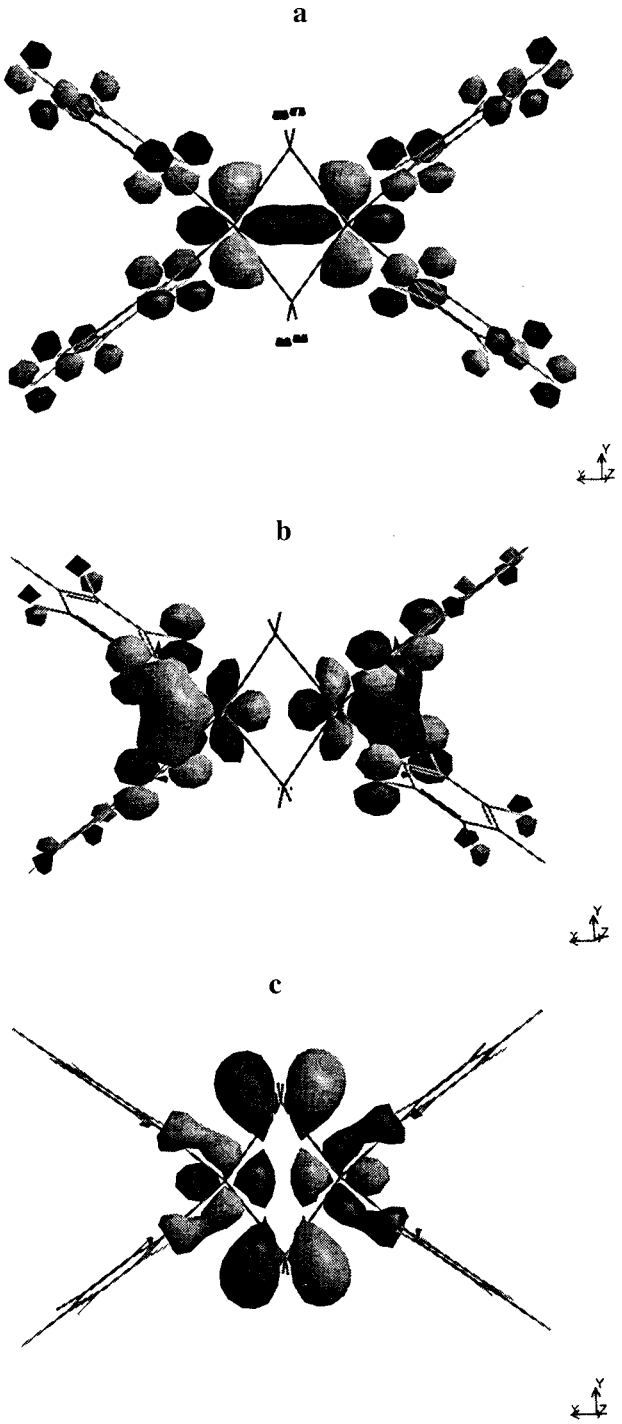

Figure 7. DFT orbital drawings for (a) the a_g (σ) orbital, (b) the b_{3u} (Pt−C bonding) orbital, and (c) the $b_{3u}(\sigma^*)$ orbital in $[Pt_2(\mu\text{-}PH_2)_2(C_6F_5)_4]$.

One of the most significant differences in the electronic structures of the two compounds is the involvement of the Pt−Pt antibonding orbital of σ^* type in metal−ligand interactions in the oxidized species. As mentioned earlier, the σ^* orbital is an antibonding combination of the metal $d_{x^2-y^2}$ orbitals and has b_{3u} symmetry. The orbitals having significant σ^* contributions are labeled in the right column of Figure 5. One of them is the occupied, low-energy b_{3u} orbital labeled as Pt−C bonding. Indeed, as shown in Figure 7b, this orbital does not display any repulsive character between the two metal atoms; rather, it

is essentially involved in the Pt−C bonding. The other b_{3u} orbital of this type, the lowest *unoccupied* orbital in the Pt_2(III,III) compound, is labeled as $b_{3u}(\sigma^*)$ in the right column of Figure 5. Besides significant contributions from the bridging phosphorus atoms, the orbital has a strong, repulsive antibonding character of σ^* type between the two metal atoms, as shown in Figure 7c. One important conclusion we may draw from the above analyses is that the Pt−Pt σ-bonding role of the $a_g(\sigma)$ orbitals is not canceled out by any significant σ^*-antibonding effects. In other words, there is approximately a single σ bond between the pair of metal atoms in the Pt_2(III,III) compound.

Finally, we point out that, in terms of the contribution of the bridging phosphorus atoms in Figure 7c, the $b_{3u}(\sigma^*)$ orbital should be correlated to the b_{3u} (Pt−P bonding) orbital of the Pt_2(II,II) compound shown in Figure 6b. They differ mainly in the types of metal orbitals that contribute to them. The b_{3u} (Pt−P bonding) orbital in the Pt_2(II,II) compound has less metal character, mainly from the 6s and 6p orbitals, as we saw previously. In the Pt_2(III,III) compound, the large contribution of the metal $d_{x^2-y^2}$ orbitals has led to a different picture of Pt−P bonding interaction in the $b_{3u}(\sigma^*)$ orbital. As shown in Figure 7c, there is actually an *antibonding* effect between the $d_{x^2-y^2}$ orbital and the phosphorus p_x orbitals in the region perpendicular but outside the Pt−Pt bond, which then leads to a diminishing Pt−P bonding character in the center part of the molecule as compared to the case in Figure 6b for the b_{3u} (Pt−P bonding) orbital.

Concluding Remarks

The one-electron oxidation (per platinum) of the dinuclear Pt(II) diamagnetic compound results in the formation of the dinuclear Pt(III) compound with formal configuration d^7. This compound is diamagnetic and the platinum centers are very close, suggesting the presence of a strong Pt−Pt bond. Theoretical calculations by density functional theory predict very well the molecular structure and suggest the existence of a σ Pt−Pt bond, which accounts for the short Pt−Pt distance in the oxidized compound.

Acknowledgment. We thank the DGICYT (Spain) for financial support (Project PB95-0003-CO2-01), the DGA for a grant (to E.A.), the Robert A. Welch Foundation for financial support, and the Supercomputing Center and the Department of Chemistry at Texas A&M University for granting computer time. We are grateful to Professor M. B. Hall for computer program access.

Supporting Information Available: For the crystal structures of compounds **1′** and **2**, tables of crystallographic data, atomic coordinates and *U*(eq) values, bond distances and angles, anisotropic displacement parameters, and H atom coordinates and *U*(eq) values. This material is available free of charge via the Internet at http://pubs.acs.org.

IC981437Z